Electrochimica Acta 173 (2015) 743–749

Contents lists available at ScienceDirect

Electrochimica Acta

journal homepage: www.elsevier.com/locate/electacta

Electrochemical production of colloidal sulphur by reduction of sulphur dioxide using a parallel plate reactor with convergent flow

J.P. Fornés, J.M. Bisang *

Programa de Electroquímica Aplicada e Ingeniería Electroquímica (PRELINE), Facultad de Ingeniería Química, Universidad Nacional del Litoral, Santiago del Estero 2829, S3000AOM Santa Fe, Argentina

ARTICLE INFO

Article history:
Received 25 February 2015
Received in revised form 18 May 2015
Accepted 20 May 2015
Available online 30 May 2015

Keywords:
colloidal sulphur
sulphur dioxide
convergent flow
electrochemical reactor
sulphur production

ABSTRACT

A parallel-plate electrochemical reactor with a double convergent flow at the cathodic and also at the anodic compartment is analysed for the production of colloidal sulphur by reduction of sulphur dioxide. A reactor with convergent flow was adopted in order to enhance the mass-transfer conditions along the electrode length. A mathematical treatment is presented for reactors with convergent flow based on the plug flow model, which can predict the maximum current. However, at higher times the cathode is blocked by the deposited sulphur decreasing the current. The best working conditions were achieved with a polished cathode working at a potential of −0.7 V against SCE for a volumetric flow rate of $8.33 \times 10^{-6}\,m^3\,s^{-1}$ obtaining $19.6\,kg\,m^{-3}\,h^{-1}$ as the maximum value of space time yield, for which the electrical parameters were 2.6 V average cell voltage, 22 kWh kg^{-1} specific energy consumption and 40 % current efficiency. The colloidal sulphur presents particles of spheroidal shape with an average diameter of 1.85 μm.

1. Introduction

Finely divided elemental sulphur suspended in water, called as colloidal sulphur, has been used traditionally as a fungicide [1,2] and pesticide. Sulphur, generally applied by spraying, has the advantage of not being consumed by the plant; residues are washed off by rain and act as a nutrient in the soil being used as a fertilizer [3]. Other users of elemental sulphur are the pharmaceutical [4], cosmetics, photographic, soap, and dye industries [5]. Nanosize sulphur particles are useful for modification of carbon nano tubes [6,7], and synthesis of nano composites for lithium batteries [8,9]. Likewise, the shape and size of sulphur particles are important factors affecting their properties and applications.

The production of colloidal sulphur can be carried out by means of physical, chemical and electrochemical procedures. The physical methods include:

(i) solvent/non-solvent precipitation process. La Mer and Dinegar [10] examined the addition of water to ethanol or acetone solutions of sulphur and Shamsipur *et al.* [11] used the systems carbon disulfide / acetone at room temperature and hot-ethanol / water.
(ii) Grinding of a sulphur slurry in a ball mill in presence of surfactants [12].
(iii) Use of amino acids as modifiers to modulate nanoparticles [13].

Chemical procedures were also proposed:

(i) Disproportion of thiosulphate in inorganic [14] or organic acid media assisted by surfactants [15].
(ii) Oxidation of sodium sulphide by air [16] or using Fe(III) as oxidizing agent in presence of chelates [17].
(iii) Reaction between sodium polysulfide and hydrochloric acid in a reverse microemulsions system [18].

Electrochemical proposals were also examined by the production of colloidal sulphur:

(i) Sodium thiosulfate is first reduced at the surface of a cathode and, in the next step, the produced sulphide ions is oxidized to elemental sulphur at the anode [11].
(ii) Oxidation of hydrogen sulphide ions to elemental sulphur at the anode coupled either to hydrogen evolution at the cathode or to oxygen reduction in a gas diffusion electrode giving a fuel cell arrangement [19].
(iii) Elemental sulphur is generated by reduction of sulphur dioxide at the cathode of an electrochemical reactor [20].

* Corresponding author.
E-mail address: jbisang@fiq.unl.edu.ar (J.M. Bisang).

http://dx.doi.org/10.1016/j.electacta.2015.05.120
0013-4686/

This strategy allows simultaneously the removal of the pollutant sulphur dioxide and its conversion to a useful chemical product.

Studies with a rotating disc electrode [20] demonstrated that: i) for a 316L stainless steel cathode at a potential of −0.5 V, against a saturated calomel electrode (SCE), the sulphur dioxide reduction occurs at limiting current conditions, ii) the high current density and the narrow range of potentials where the limiting current is observed suggest that this reaction can be carry out in reactors with a bi-dimensional cathode and iii) at potentials more negative than −0.5 V, hydrogen evolution also takes place and the current efficiency for sulphur production diminishes. On the other hand, hydrogen evolution has two beneficial effects given by the increase of the mass-transfer by bubble induced convection and assists in dislodging the sulphur layer from the cathode.

Electrochemical reactors with parallel-plate electrodes are the most widespread configuration used in the industrial practice and its versatility has been fully demonstrated [21]. Moreover, when the reaction of interest is under mass-transfer control a strategy to enhance the reactor performance is the use of a convergent channel [22], where a continuous reduction in the cross-section area for the solution flow is used as a means of improving mass-transfer in a parallel plate electrochemical reactor. Depending on the operating conditions, the convergent flow increases the mean mass-transfer coefficient by 10-60% and mass-transfer distribution under laminar flow becomes more uniform. The aim of this paper is to examine the behaviour of a parallel-plate electrochemical reactor with a double convergent channel for the electrosynthesis of colloidal sulphur by reduction of sulphur dioxide operating at limiting current conditions.

2. Experimental

The reactor was made of acrylic material, 100 mm wide and 270 mm long as inner dimensions, arranged in a filter press configuration. The complete experimental arrangement is schematically depicted in Fig. 1. A graphite sheet, grade 6503Carbone Lorraine (Mersen, Buenos Aires, Argentina), 10 mm thick, was used as anode and it was electrically fed in its backside by means of three threaded screws of stainless steel. The graphite anode supports a GF-S4 graphite felt, 0.3 mm thick, supplied by The Electrosynthesis Co., Inc. (Lancaster, NY, USA) in order to increase the anodic surface area. The cathode was a sheet of 316 stainless steel, 0.5 mm thick, electrically connected along its two lateral sides by means of copper current feeders, which were joined to the dc power supply at both ends to ensure isopotentiality of the metal phase. The geometric surface area of the cathode was 235.7 cm^2. The anodic and cathodic compartments were separated by a sheet of microporous polyethylene (Daramic Industrial CL, Charlotte, NC, USA), 0.4 mm backweb thickness and 58% porosity, in order to avoid the deactivation of the anode by the elemental sulphur cathodically produced [20]. Each compartment presents at its ends chambers of a triangular cross-sectional area, which were filled with expanded plastic meshes to homogenize the flow. Fig. 1 part (b) shows an exploded view of the inlet chamber in the anodic compartment, the cathodic outlet chamber is similar, and Fig. 1 part (c) represents the distribution chamber of electrolyte at each compartment. The solid and dashed arrows represent the electrolyte flow at the anodic and cathodic compartments, respectively. Thus, the solution was fed in the inlet chamber of the anodic compartment by means of a perpendicular nozzle. The double convergent channel inside the anodic compartment was achieved by using a gasket of the appropriate shape as it is shown

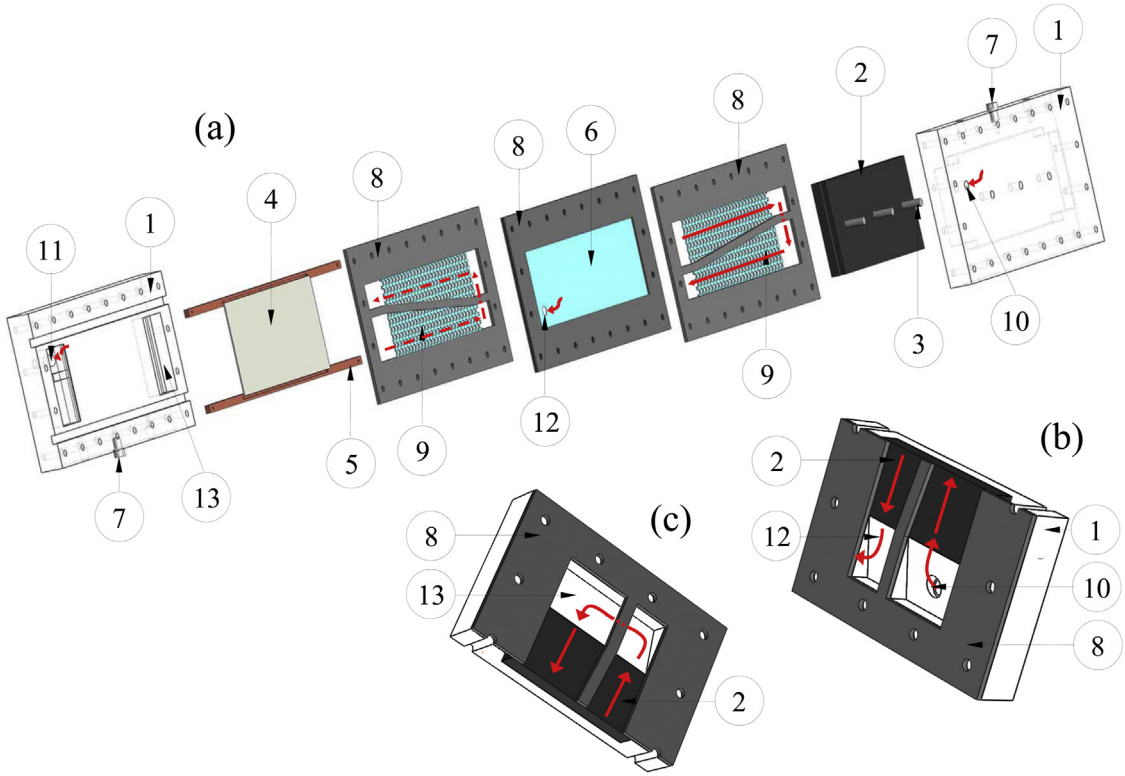

Fig. 1. (a) Schematic representation of the parallel plate electrochemical reactor with convergent flow. (b) Exploded view showing the electrolyte inlet chamber in the anodic compartment. (c) Exploded view showing the final electrolyte distribution chamber at each compartment. (1) plates; (2) anode; (3) current feeders to the anode; (4) cathode; (5) current feeders to the cathode; (6) separator; (7) connexion to Luggin capillaries; (8) gaskets; (9) expanded plastic meshes; (10) electrolyte inlet; (11) electrolyte outlet; (12) electrolyte connexion between anodic and cathodic compartments through a hole in the separator; (13) electrolyte distribution chambers. Solid arrows: electrolyte flow in the anodic compartment. Dashed arrows: electrolyte flow in the cathodic compartment.

in Fig. 1 part (a). The width of each convergent channel is 54.3 mm at the inlet and 33 mm at the outlet, giving a convergence ratio of 0.4. The solution enters to the inlet chamber of the cathodic compartment through a hole in the separator and makes also a double convergent flow in it. The interelectrode gap at each compartment was 2.0 mm, which was fixed by the thickness of the gasket. The anodic and cathodic interelectrode gaps were filled with expanded plastic meshes, summarized in Table 1, whose turbulence promotion action becomes more uniform the mass-transfer conditions along the electrode length [23]. The turbulence promoter EPM2 was used in the cathodic compartment and the EPM1 in the anodic part.

The following reactions occur at the cathode [20]

$$SO_2 + 4\ H^+ + 4\ e^- \rightarrow S + 2\ H_2O \tag{1}$$

and

$$SO_2 + 6\ H^+ + 6\ e^- \rightarrow H_2S + 2\ H_2O \tag{2}$$

Combining Eqs. (1) and (2) results in

$$\left(1+\frac{\beta_c}{2}\right)SO_2 + 6H^+ + 6e^- \rightarrow \frac{3\beta_c}{2}S + (1-\beta_c)\ H_2S + (2+\beta_c)\ H_2O \tag{3}$$

where β_c is the current efficiency for the sulphur production. At the anode takes place the oxidation of sulphur dioxide to sulphuric acid, according to

$$SO_2 + 2\ H_2O \rightarrow HSO_4^- + 3H^+ + 2\ e^- \tag{4}$$

Adding Eqs. (3) and (4) yields

$$\left(4+\frac{\beta_c}{2}\right)\ SO_2 + (4-\beta_c)\ H_2O \xrightarrow{6F} \frac{3\beta_c}{2}S + (1-\beta_c)\ H_2S + 3\ H_2SO_4 \tag{5}$$

which represents the overall reaction for the electrochemical reactor, being F the Faraday constant. Eq. (5) also shows that the pH change of the solution at the reactor outlet is only attributable to the sulphuric acid anodically generated. The oxidation at the anode of the hydrogen sulphide, cathodically produced, is not thermodynamically favoured. The formation of hydrogen sulphide as an undesirable side cathodic product requires the implementation of a process for treating this effluent [19] in large-scale electrolysis.

The experiments were carried out potentiostatically. The cathodic potential was controlled against SCE, connected to a Haber-Luggin capillary positioned in the middle region of the cathode. The anodic potential was also measured using a Haber-Luggin capillary also positioned in its middle region. During the experiment the cell voltage, the current and the anodic potential were recorded as a function of time. Only one pass of the solution through the reactor was allowed. Then, the reactor was made part of a flow circuit system consisting of a pump, a flow meter, initial and final reservoirs, and connections to maintain the temperature at the preset value, 30 °C.

Table 1
Geometrical parameters of the turbulence promoters.

Characteristic parameters of the expanded plastic mesh (EPM)	EPM1	EPM2
Long diagonal, / mm	21	16.2
Short diagonal, / mm	5.5	11.5
Long mesh aperture, / mm	12.5	11.0
Short mesh aperture, / mm	3	9.5
Thickness, / mm	1.2	0.5
Apparent thickness, (1 sheet) / mm	2.4	1.2
Strand width, / mm	1.8	1.0
Specific surface area, / m^{-1}	1015	571
Porosity, ε	0.67	0.85

Table 2
Physicochemical properties of the electrolyte.

Composition	$[SO_2] \cong 5\ g\,dm^{-3}$ in $0.1\ mol\,dm^{-3}\ H_2SO_4$
ν / $m^2\,s^{-1}$	1.07×10^{-6}
D / $m^2\,s^{-1}$	1.53×10^{-9}
Sc	699

Experiments were performed using a solution of $5\ g\,dm^{-3}\ SO_2$ in $0.1\ mol\,dm^{-3}\ H_2SO_4$ as supporting electrolyte, prepared dissolving sodium sulphite in an aqueous solution of sulphuric acid to achieve the above concentrations. Table 2 summarizes the composition and physicochemical properties of the solution, which were measured in the laboratory. At the end of the experiment the sulphur was left to precipitate. The solution was taken out and the amount of elemental sulphur in the precipitate was determined according to the method described by Morris *et al.* [24]. Thus, sulphur was oxidized to thiosulphate by boiling in a sodium sulphite solution, the excess of sulphite was bound with formaldehyde and the thiosulphate was determined by iodometric titration. The efficiency of the anode was not analysed because the change in the sulphuric acid concentration is undetectable for one pass of the solution through the anodic compartment.

3. Residence time distribution study

The hydrodynamic behaviour of electrochemical reactors is usually characterized by means of the stimulus-response method and it is reported the normalized outlet concentration, termed E curve [25], defined as

$$E(t) = \frac{c(t,1)}{\int_0^\infty c(t,1)\mathrm{d}(t/t_{mean})} \tag{6}$$

being $c(t,1)$ the outlet concentration, t the time and t_{mean} is calculated as

$$t_{mean} = \frac{\int_0^\infty tc(t)\mathrm{d}t}{\int_0^\infty c(t)\mathrm{d}t} \tag{7}$$

The correlation of the experimental residence time distributions was made by using

$$E = \sqrt{\frac{Pe}{4\pi T^3}}e^{-\left[\frac{Pe(1-T)^2}{4T}\right]} \tag{8}$$

which is supposed to be valid for converging flow. Here, the Peclet number, Pe, is introduced as a global parameter to evaluate the dispersion in the reactor, defined as:

$$Pe = \frac{u_{av}L}{\varepsilon D_L} \tag{9}$$

where u_{av} is the average superficial liquid flow velocity in the reactor, D_L is the dispersion coefficient and ε is the porosity. For Pe numbers higher than 5, Eq. (8) is appropriate to fit experimental results [26]. The dimensionless time, T, is given by

$$T = \frac{t}{t_{mean}} \tag{10}$$

Fig. 2 shows a typical residence time distribution for the reactor, obtained by using the stimulus-response method. As a stimulus, an impulse function was simulated by manually injecting a 30 wt% NaOH solution, 1 cm^3, into the inlet for a short time. The full line corresponds to experimental results of five independent experiments, where it can be observed a main peak giving an acceptable hydrodynamic behaviour of the reactor. The dashed line represents their correlation by means of a weighted least square

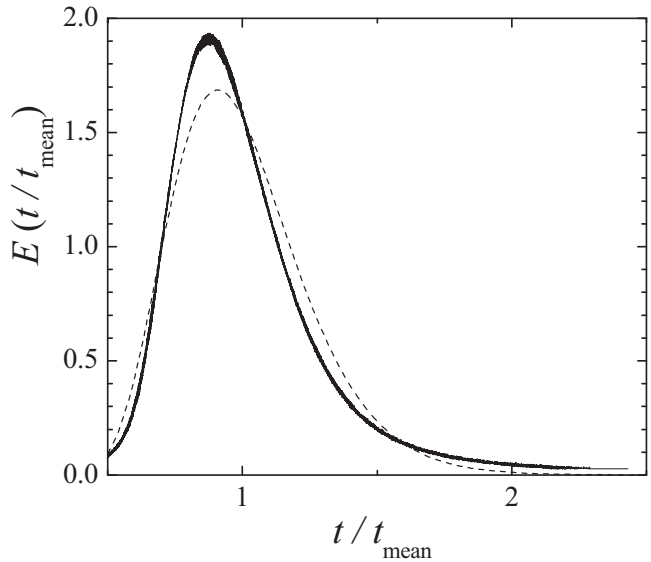

Fig. 2. Comparison of experimental and theoretical residence time distributions. Full lines: experimental. Dashed line: theoretical according to Eq. (8). $Q = 8.33 \times 10^{-6}\,m^3\,s^{-1}$.

method applied to Eq. (8) using the Peclet number as fitting parameter. The mean square error, MSE, was used to quantify the agreement, given by

$$\mathrm{MSE} = \frac{1}{N-1}\sum_{i=1}^{N}\gamma_i(E_i^{th} - E_i^{exp})^2 \tag{11}$$

where N is the number of experimental data and the subscripts "exp" and "th" denote the experimental and theoretical values, respectively. The weighted factor is

$$\gamma_i = \frac{E_i^{exp}}{E_{mean}^{exp}} \tag{12}$$

The Peclet number for which MSE is minimal is then taken as the best fit value. Table 3 summarizes the results. The Peclet number is always higher than 20, which validate the use of Eq. (8) to fit the experimental results and for this value of the Peclet number the behaviour of the reactor is close to that given by the plug flow model.

4. Mathematical model

Assuming the plug flow model in the convergence channel, the mass-balance yields

$$dc = -\frac{k_{m,y}c}{Q}dA \tag{13}$$

here c is the concentration, Q is the volumetric flow rate and $k_{m,y}$ is the local mass-transfer coefficient, which depends on the position along the electrode length [22]. For simplicity, in the following a mean mass-transfer coefficient, k_m, is used. The electrode surface area, A, is given by

Table 3
Summary of results related to residence time distribution.

$Q \times 10^6$ ($m^3\,s^{-1}$)	t_{mean} (s^{-1})	Pe	MSE
3.3	48.7	24	0.0530
5.0	34.8	26	0.0487
8.3	22.5	31	0.0222
13.3	16.2	30	0.0859

$$dA = W(0)\left(1 - \frac{\lambda y}{L}\right)dy \tag{14}$$

being $W(0)$ the channel width evaluated at the inlet, y the axial coordinate along the electrode, L the electrode length and λ the convergence ratio, defined as

$$\lambda = 1 - \frac{W(L)}{W(0)} \tag{15}$$

Combining Eqs. (13), (14) and (15), after integration the concentration along the electrode length results in

$$c(y) = c(0)\exp\left[-\xi\frac{y}{L}\left(1 - \frac{\lambda y}{2L}\right)\right] \tag{16}$$

Here ξ is a dimensionless number which lumps the mean mass-transfer coefficient, geometric electrode parameters with the volumetric flow rate, defined as

$$\xi = \frac{k_m W(0) L}{Q} \tag{17}$$

Evaluating Eq. (16) at $y = L$, the concentration at the outlet of a convergent channel is given by

$$c(1) = c(0)\exp\left[-\xi\left(1 - \frac{\lambda}{2}\right)\right] \tag{18}$$

Analogously, in case of n convergent channels connected in series the outlet concentration is

$$c(n) = c(0)\exp\left[-n\xi\left(1 - \frac{\lambda}{2}\right)\right] \tag{19}$$

Likewise, the current balance, I, is given by

$$dI = \nu_e F k_m c(y) dA \tag{20}$$

being ν_e the number of electrons interchanged and F the Faraday constant. Introducing Eq. (14) and Eq. (16) into Eq. (20), after integration the current at a convergent channel results in

$$I = \nu_e F Q c(0)\left\{1 - \exp\left[-\xi\left(1 - \frac{\lambda}{2}\right)\right]\right\} \tag{21}$$

Analogously, in case of n convergent channels connected in series the total current is

$$I(n) = \nu_e F Q c(0)\left\{1 - \exp\left[-n\xi\left(1 - \frac{\lambda}{2}\right)\right]\right\} \tag{22}$$

Likewise, the mean mass-transfer coefficient for a convergent channel is given by [22]

$$\mathrm{Sh} = 1.232\left[\mathrm{Re}(0)\mathrm{Sc}\frac{d_h}{L}\right]^{1/3}\Psi(\lambda) \tag{23}$$

being

$$\Psi(\lambda) = \frac{B_{\lambda/2}(2/3, 2/3) - 2B_{\lambda/2}(5/3, 2/3)}{(1 - \lambda/2)(\lambda/2)^{2/3}} \tag{24}$$

where $B_{\lambda/2}(2/3, 2/3)$ and $B_{\lambda/2}(5/3, 2/3)$ are the incomplete Beta function defined as

$$B_\omega(a, b) = \int_0^\omega t^{a-1}(1-t)^{b-1}dt \tag{25}$$

For $\lambda = 0.4$ is $\Psi(0.4) = 1.6158$. The Sherwood number, Sh, the Reynolds number evaluated at the reactor inlet, Re(0), and the Schmidt number, Sc, are defined as

$$\mathrm{Sh} = \frac{k_m d_h}{D} \tag{26}$$

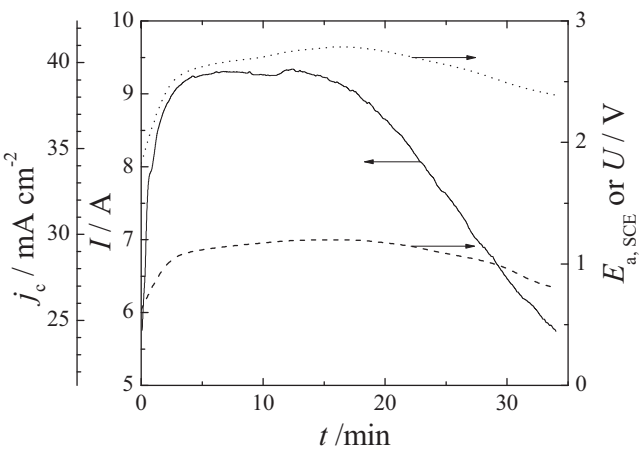

Fig. 3. Electrical variables as a function of time. Full line: total current, I or cathodic current density, j_c. Dashed line: anodic potential, $E_{a,SCE}$. Dotted line: cell voltage, U. $E_{c,SCE} = -0.7$ V. $Q = 8.33 \times 10^{-6}$ m^3 s^{-1}. $T = 30$°C.

$$\mathrm{Re}(0) = \frac{u(0)d_h}{\nu} \tag{27}$$

and

$$\mathrm{Sc} = \frac{\nu}{D} \tag{28}$$

here d_h is the hydraulic diameter, calculated as two times the interelectrode gap, D is the diffusion coefficient and ν is the kinematic viscosity.

5. Results and discussion

Fig. 3 shows the total current or the cathodic current density, j_c, the anodic potential, $E_{a,SCE}$, and the cell voltage, U, as a function of time for a typical experiment. The cathode was polished with emery paper up to grade 2500. It can be observed that after a short activation time the current achieves a limiting value and diminishes at higher times due to the blocking of the cathode surface by the deposited sulphur. The anodic potential and the cell voltage show a similar tendency that the current but less marked. Likewise, the anodic potential is always lower than 1.5 V hindering the oxygen evolution as side anodic reaction [20]. Table 4 reports on theoretical values for the reactor with a polished cathode for experiments at different volumetric flow rates and also compares the experimental and theoretical currents. In the theoretical calculation 5 was assumed as the number of exchanged electrons per sulphur dioxide molecule, which results from Eq. (3) with a cathodic current efficiency of 40%, as it is declared later. The fourth and fifth columns show the theoretical sulphur dioxide concentration, according to Eq. (19), in the inlet and outlet of the cathodic compartment, respectively. The sixth and seventh columns compare the theoretical and experimental currents, where it can be observed that the predicted value, Eq. (22), is similar to the maximum measured one. The difference between both can be explained taking into account that the mass-transfer coefficient was estimated with Eq. (23), and the effects of the gas-bubble convection due to hydrogen evolution and the turbulence promotion by the expanded plastic mesh in the interelectrode gap were disregarded in the calculation, which enhance the mass-transfer of sulphur dioxide at the cathode.

Table 4
Summary of results of colloidal sulphur production at a polished cathode.

$Q \times 10^6$ / m^3 s^{-1}	$k_m \times 10^6$ Eq. (23) / m s^{-1}	$\xi \times 10^2$	c_i / g dm^{-3}	c_o / g dm^{-3}	I_{th} / A	I_{exp} / A
4.17	8.69	3.055	4.76	4.53	7.17	7.8
8.33	10.95	1.925	4.85	4.70	9.28	9.3
11.33	12.13	1.568	4.88	4.75	10.37	12.9

Solution at the reactor inlet: 5 g dm^{-3} SO_2 in 0.1 mol dm^{-3} H_2SO_4 as supporting electrolyte. $E_{c,SCE} = -0.7$ V. $T = 30$ °C. c_i and c_o: theoretical inlet and outlet concentrations of sulphur dioxide at the cathodic compartment according to Eq. (19). I_{th}: theoretical current according to Eq. (22). I_{exp}: maximum in the experimental current.

Fig. 4 compares the variation of the current with time for two experiments with the cathode in different initial state and on the right axis the cathodic current density is also shown. Thus, the dashed line corresponds to the cathode polished with emery paper, similar to Fig. 3, whereas for the full line the cathode of a previous experiment was only brushed to remove partially the deposited sulphur. The brushed cathode drains at the beginning of the experiment a lower current than that of the polished electrode because the sulphur blocks the surface area of the electrode. However, at high times both electrodes give approximately the same current, which is about half of the maximum value measured at the polished electrode. Then, the deposited sulphur blocks an important part of the cathode surface. The oscillations in the current can be explained taking into account two opposite effects: i) hydrogen evolution detaches the deposited sulphur increasing the current and ii) new sulphur clusters produced at the cathode cover its surface decreasing the current. This behaviour is more marked for the brushed cathode which is initially covered with a thin layer of sulphur. The second effect predominates on the first and the current diminishes with time.

Fig. 5 reports on the figures of merit of the reactor for the production of colloidal sulphur as a function of the potential applied to the cathode when the electrode was polished with emery paper. As expected, an increase in the cell voltage, U, and in the specific energy consumption, E_s, and a decrease in the current efficiency, β_c, is observed when the cathodic potential becomes more negative. This behaviour is a consequence of hydrogen evolution as side cathodic reaction. However, the space time yield, ρ, shows a relative maximum at a potential of −0.7 V. The same performance was observed with a rotating cylinder electrode [20], which can be explained taking into account that hydrogen evolution improves the mass-transfer at the cathode surface enhancing the formation of colloidal sulphur and removing the

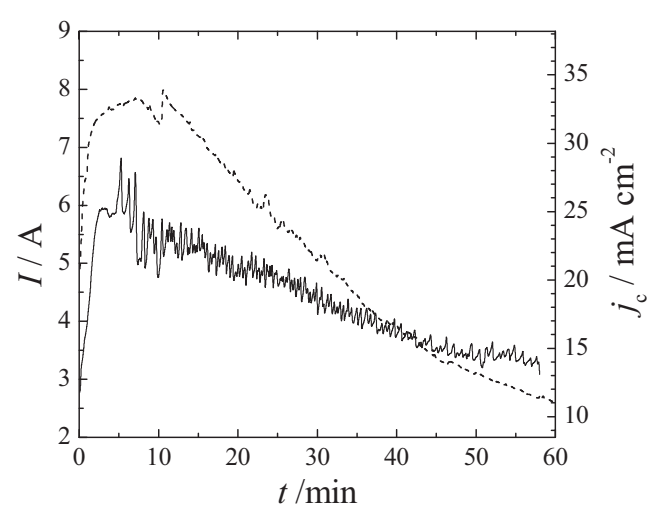

Fig. 4. Current and cathodic current density as a function of time. Full line: cathode brushed from a previous experiment. Dashed line: cathode polished with emery paper. $E_{c,SCE} = -0.7$ V. $Q = 4.17 \times 10^{-6}$ m^3 s^{-1}. $T = 30$°C.

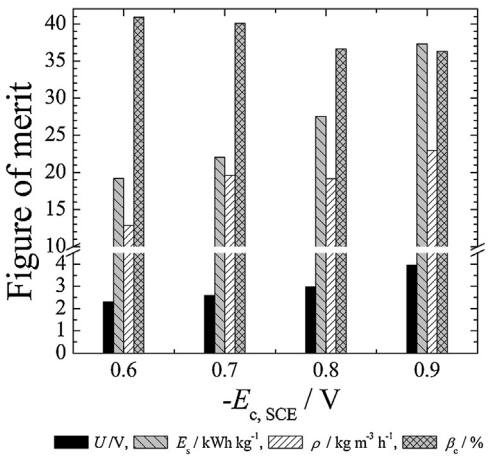

Fig. 5. Figures of merit for the colloidal sulphur production at a 316 stainless steel cathode as a function of the cathodic potential. Cathode polished with emery paper. 5 g dm^{-3} SO_2 in 0.1 mol dm^{-3} H_2SO_4 as supporting electrolyte. $Q = 8.33 \times 10^{-6}$ m^3 s^{-1}. $T = 30$ °C. *U*, cell voltage; E_s, specific energy consumption; ρ, space time yield; β_c, current efficiency.

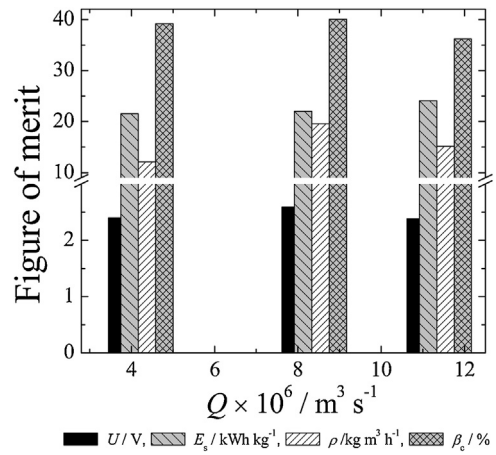

Fig. 7. Figures of merit for the colloidal sulphur production at a 316 stainless steel cathode as a function of the volumetric flow rate. Cathode polished with emery paper. 5 g dm^{-3} SO_2 in 0.1 mol dm^{-3} H_2SO_4 as supporting electrolyte. $E_{c,SCE} = -0.7$ V. $T = 30$ °C. *U*, cell voltage; E_s, specific energy consumption; ρ, space time yield; β_c, current efficiency.

sulphur deposited on it. However, at more cathodic potentials hydrogen evolution predominates over sulphur production and the space time yield diminishes. Then, it is corroborated that −0.7 V represents an optimal value for the cathodic potential. It must be remarked that the experiment carried out at − 0.9 V shows a slight improvement of the space time yield but with a strong increase in the specific energy consumption. Likewise, in this experiment the anodic potential was higher than 1.5 V and oxygen evolution also takes place at the anode as side reaction.

Figs. 6 and 7 show the figures of merit of the reactor for the production of colloidal sulphur as a function of the volumetric flow rate when the electrode is brushed or polished, respectively. Both figures demonstrate that for a volumetric flow rate of 8.33×10^{-6} m^3 s^{-1} is achieved the maximum values of space time yield and current efficiency with a minimum in the specific energy consumption. This optimal volumetric flow rate is the consequence of two opposite effects. In the first place an increase in the volumetric flow rate facilitates the removal of the hydrogen evolved at the cathode, which can block the cathodic surface area hindering the formation of colloidal sulphur. But in the second place, the conversion per pass diminishes with the increase in the volumetric flow rate. This effect predominates on the first giving an optimal volumetric flow rate, for which the figures of merit of the reactor are: 2.6 V average cell voltage, 22 kWh kg^{-1} specific energy consumption, 40 % current efficiency and 19.6 kg m^{-3} h^{-1} for the space time yield when the potential is −0.7 V at a polished cathode.

6. Morphological characterization of the colloidal sulphur

The colloidal sulphur obtained at a volumetric flow rate of 8.33×10^{-6} m^3 s^{-1}, $E_{c,SCE} = -0.7$ V at a polished cathode was separated from the solution by sedimentation. The product was dried in a desiccator over silica gel and its surface morphology was examined by scanning electron microscopy. Fig. 8 shows a micrograph of the colloidal sulphur with spheroidal particles and the inset in the upper-right corner reports on the sulphur

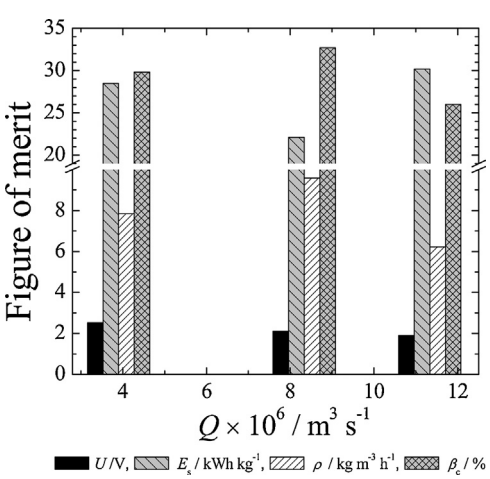

Fig. 6. Figures of merit for the colloidal sulphur production at a 316 stainless steel cathode as a function of the volumetric flow rate. Cathode brushed. 5 g dm^{-3} SO_2 in 0.1 mol dm^{-3} H_2SO_4 as supporting electrolyte. $E_{c,SCE} = -0.7$ V. $T = 30$ °C. *U*, cell voltage; E_s, specific energy consumption; ρ, space time yield; β_c, current efficiency.

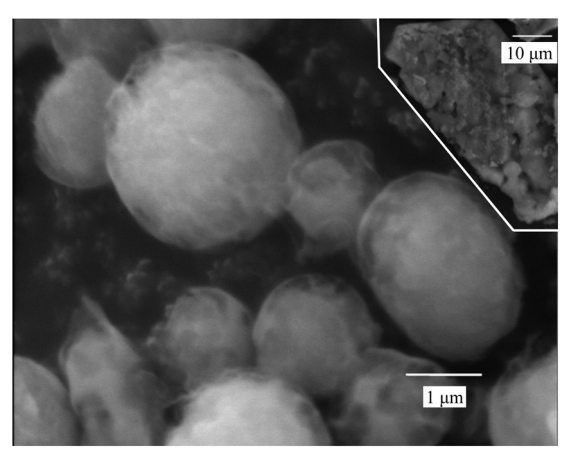

Fig. 8. Scanning electron micrograph of colloidal sulphur. Magnification: ×6000. Inset: Micrograph of the sulphur detached from the cathode. Magnification: ×2000. $Q = 8.33 \times 10^{-6}$ m^3 s^{-1}, $E_{c,SCE} = -0.7$ V. $T = 30$ °C.

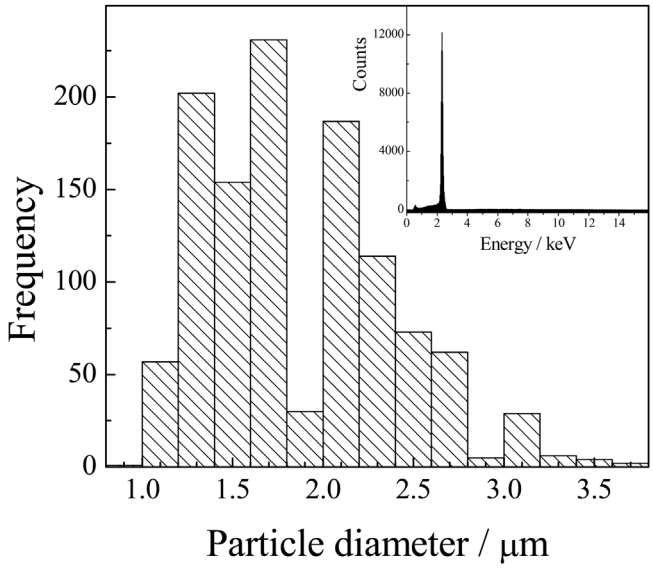

Fig. 9. Distribution of the diameter of the colloidal sulphur particles. Inset: EDAX spectrum of the colloidal sulphur. Q =8.33 × 10^{-6} $m^3 s^{-1}$, $E_{c,SCE}$ =−0.7 V. T = 30°C.

detached from the cathode, where it can be observed the coalescence of the spheroids of sulphur forming platelets and blocking the cathode surface area. Fig. 9 shows the histogram of the diameter for the spheroidal particles of colloidal sulphur obtained in the experiment of Fig. 8. The particle diameter is in the range from 1.1 μm to 2.7 μm with a mean value of 1.85 μm and a standard deviation of 0.51 μm, showing that all the particles present a similar size. The composition of the colloidal sulphur and also of the sulphur detached from the cathode was determined by EDAX and the inset in Fig. 9 reports on a typical spectrum, where the characteristic peaks corresponding to sulphur are only detected giving a product of high purity.

7. Conclusions

The use of a divided electrochemical reactor with parallel-plate electrodes and a double convergent flow in both compartments, anodic and cathodic, has allowed the synthesis of colloidal sulphur by reduction of sulphur dioxide from an acid solution. The particles are of high purity, spheroidal shape with a size in the range from 1.1 μm to 2.7 μm. Sulphur is also deposited at the cathode, blocking the electrode surface area and diminishing the current close to half of the theoretical value. This points to the need to search for methods or strategies to remove the deposited sulphur.

Acknowledgements

This work was supported by the Agencia Nacional de Promoción Científica y Tecnológica (ANPCyT), Consejo Nacional de Investigaciones Científicas y Técnicas (CONICET) and Universidad Nacional del Litoral (UNL) of Argentina.

References

[1] M.A. Ellis, D.C. Ferree, R.C. Funt, L.V. Madden, Effects of an apple scab-resistant cultivar on use patterns of inorganic and organic fungicides and cconomics of disease control, Plant Disease 82 (1998) 428.
[2] S.R. Choudhury, K.K. Nair, R. Kumar, R. Gogoi, C. Srivastava, M. Gopal, B.S. Subhramanyam, C. Devakumar, A. Goswami, Nanosulfur: a potent fungicide against food pathogen Aspergillus niger, AIP Conference Proceedings 1276 (2010) 154.
[3] C.C. Boswell, D.K. Friesen, Elemental sulfur fertilizers and their use on crops and pastures, Fertilizer Research 35 (1993) 127.
[4] A.N. Lin, R.J. Reimer, D.M. Carter, Sulfur revisited, Journal of the American Academy of Dermatology 18 (1988) 553.
[5] J.A. Ober, Materials flow of sulfur, http://pubs.usgs.gov/of/2002/of02-298/
[6] J. Barkauskas, R. Juškėnas, V. Milerienė, V. Kubilius, Effect of sulfur on the synthesis and modification of carbon nanostructures, Materials Research Bulletin 42 (2007) 1732.
[7] J.M. Romo-Herrera, B.G. Sumpter, D.A. Cullen, H. Terrones, E. Cruz-Silva, D.J. Smith, V. Meunier, M. Terrones, An atomistic branching mechanism for carbon nanotubes: sulfur as the triggering agent, Angewandte Chemie International Edition 47 (2008) 2948.
[8] X. Yu, J. Xie, J. Yang, K. Wang, All solid-state rechargeable lithium cells based on nano-sulfur composite cathodes, Journal of Power Sources 132 (2004) 181.
[9] T. Kobayashi, Y. Imade, D. Shishihara, K. Homma, M. Nagao, R. Watanabe, T. Yokoi, A. Yamada, R. Kanno, T. Tatsumi, All solid-state battery with sulfur electrode and thio-LISICON electrolyte, Journal of Power Sources 182 (2008) 621.
[10] V.K. LaMer, R.H. Dinegar, Theory, production and mechanism of formation of monodispersed hydrosols, Journal of the American Chemical Society 72 (1950) 4847.
[11] M. Shamsipur, S. Pourmortazavi, M. Roushani, I. Kohsari, S.S. Hajimirsadeghi, Novel approach for electrochemical preparation of sulfur nanoparticles, Microchimica Acta 173 (2011) 445.
[12] B.M. Choudary, Z. Jamil, An economical industrial method for the manufacture of colloidal sulphur, Chemistry and Industry 1 (1986) 788.
[13] X.-Y. Xie, W.-J. Zheng, Y. Bai, J. Liu, Cystine modified nano-sulfur and its spectral properties, Materials Letters 63 (2009) 1374.
[14] V.K. LaMer, A.S. Kenyon, Kinetics of the formation of monodispersed sulfur sols from thiosulfate and acid, Journal of Colloid Science 2 (1947) 257.
[15] R.G. Chaudhuri, S. Paria, Synthesis of sulfur nanoparticles in aqueous surfactant solutions, Journal of Colloid and Interface Science 343 (2010) 439.
[16] G. Chiu, E.J. Meehan, Monodisperse sulfur sols from the air oxidation of hydrogen sulfide solutions, Journal of Colloid and Interface Science 62 (1977) 1.
[17] A.S. Deshpande, R.B. Khomane, B.K. Vaidya, R.M. Joshi, A.S. Harle, B.D. Kulkarni, Sulfur nanoparticles synthesis and characterization from H_2S gas, using novel biodegradable iron chelates in W/O microemulsion, Nanoscale Research Letters 3 (2008) 221.
[18] Y. Guo, J. Zhao, S. Yang, K. Yu, Z. Wang, H. Zhang, Preparation and characterization of monoclinic sulfur nanoparticles by water-in-oil microemulsions technique, Powder Technology 162 (2006) 83.
[19] G.H. Kelsall, Electrochemical removal of H_2S, in: G. Kreysa, K.-i Ota, R.F. Savinell (Eds.), Encyclopedia of Applied Electrochemistry, Springer, New York, 2014, pp. 593.
[20] J.P. Fornés, G.A. González, J.M. Bisang, Electrochemical conversion of sulfur dioxide with a rotating cylinder electrode working as anode or cathode, Journal of Chemical Technology and Biotechnology (2014) , doi:http://dx.doi.org/10.1002/jctb.4567 (in press).
[21] D. Pletcher, F.C. Walsh, Industrial Electrochemistry, 2nd ed, Chapman and Hall, London, 1993.
[22] A.N. Colli, J.M. Bisang, Mass-transfer characterization in a parallel-plate electrochemical reactor with convergent flow, Electrochimica Acta 113 (2013) 575.
[23] A.N. Colli, R. Toelzer, M.E.H. Bergmann, J.M. Bisang, Mass-transfer studies in an electrochemical reactor with a small interelectrode gap, Electrochimica Acta 100 (2013) 78.
[24] H.E. Morris, R.E. Lacombe, W.H. Lane, Quantitative determination of elemental sulfur in aromatic hydrocarbons, Analytical Chemistry 20 (1948) 1037.
[25] P.V. Danckwerts, Continuous flow systems. Distribution of residence times, Chemical Engineering Science 2 (1953) 1.
[26] A.N. Colli, J.M. Bisang, Evaluation of the hydrodynamic behaviour of turbulence promoters in parallel plate electrochemical reactors by means of the dispersion model, Electrochimica Acta 56 (2011) 7312.